Surface diffusion of oxygen transport membrane materials studied by grain boundary grooving

M.G. Sahini, M.-A. Einarsrud and T. Grande[1]

Department of Materials Science and Engineering,

NTNU Norwegian University of Science and Technology

NO-7491 Trondheim, Norway

Abstract

Mass transport mechanism responsible for grain boundary grooving during thermal annealing of polished ceramics of $Ba_{0.5}Sr_{0.5}Co_{0.8}Fe_{0.2}O_{3-\delta}$ (BSCF) and $La_2NiO_{4+\delta}$ (LN) was revealed by atomic force microscopy. Surface diffusion mechanism was confirmed for both materials by the evolution of the grain boundary width (w) with annealing time (t), and the surface diffusion coefficient was determined from the slope of w versus $t^{1/4}$ following the theory by Mullins. An Arrhenius temperature dependence of the surface diffusion was observed, and the activation energy was determined to be 220 ± 30 and 450 ± 30 kJ/mol respectively for BSCF and LN. The surface diffusion data is discussed with respect to similar data for other oxide materials and cation and oxygen anion diffusion in BSCF and LN. Finally, the dihedral angle for both LN and BSCF was determined, and these are typical in the range reported for other oxide materials.

[1] Corresponding author: grande@ntnu.no

Introduction

Surface diffusion plays an important role in various processes such as crystal and film growth, phase transformation, coarsening, catalysis and surface reactions.[1] The increasing importance of miniaturization in various technological devices results in an increase in surface to volume ratio and, hence, exerting significant contribution of surface properties of materials.[2] In processing of oxide materials, for example, surface diffusion can provide contribution to the processes such as coarsening, pore migration and coalescence, as well as grain growth.[3,4] The first studies of surface diffusion were conducted on a macroscopic scale at temperatures near the melting point of materials.[5] Later development of microscopic techniques allowed the study of surfaces at the atomic scale.[6-9] Radioactive tracer method has also been used, which involves spreading of tracer element over the surface followed by determination of the concentration profile of the tracer.[10]

Surface diffusion has also been conducted by mass transfer methods which involves the investigation of different surface profiles such as the decay of grain boundary, single scratch, and multiple scratches or sinusoidal profiles.[11] The grain boundary groove method, as well as creation and analysis of the surface scratch by atomic force microscopy,[12-14] have provided further improvement of the quantitative study of surface diffusion. In this method the evolution of grain boundary groove with annealing temperature and time is monitored, and the width of the groove is measured. The theory of the quantitative analysis of grain boundary grooving was developed by Mullins in the late 1950s[15] assuming the material to be isotropic. The formation of grain boundary groove was assumed to occur predominantly by surface diffusion, driven by gradient in surface curvature. This was later proved experimentally for the grain boundary groove smaller than ~10 μm.[16]

Here we present an investigation of surface diffusion of two oxygen transport membrane materials $La_2NiO_{4+\delta}$ (LN) and $Ba_{0.5}Sr_{0.5}Co_{0.8}Fe_{0.2}O_{3-\delta}$ (BSCF) by the grain boundary grooving approach using atomic force microscopy (AFM). To our knowledge, there is no surface diffusion data available for these two or other similar materials. Taking into consideration that the dihedral angle, and hence the grain boundary width is affected by crystallographic orientations, two materials with different crystal structures were considered in this study. While BSCF exhibits a perovskite crystal structure,[17] La_2NiO_4 belongs to a group of perovskite related compounds called Ruddlesden Popper series, having $LaNiO_3$ perovskite layers alternating with LaO rock salt – type layers along the c-crystallographic orientation.[18]

Surface diffusion by grain boundary grooving: Methodology

The theory of the grain boundary grooving is based on the work by Mullins.[15,16] The width of the grain boundary groove, w, is defined by the equation:

$$w = 4.6(Bt)^{1/4} \tag{1}$$

in which

$$B = \frac{D_s \gamma \Omega^2 N}{kT} \tag{2}$$

where D_s is the surface diffusion coefficient, γ is the surface free energy, Ω is the molecular volume of the diffusing species and N is number of molecules/cm^2 of the surface. N is defined by $N = \Omega^{-2/3}$.

Experimental data on surface energy are rarely reported, and no such data are available for BSCF or LN. A density functional theory study has reported 0.51 Jm^{-2} for (100) surface[19], while in an earlier theoretical work values from 0.98 to 1.69 was reported dependent on the crystallographic orientation[20]. Corresponding data for BSCF are not available, but a recent review on first principle studies of related II-IV perovskite materials with Ba or Sr on A-site reveal that the surface energy vary typically in the range 1-4 Jm^{-2} with values close to 1 for the most stable (100) surfaces[21,22]. Based on these reports we have used a temperature independent surface diffusion of 1 Jm^{-2} in this work.

The diffusion species for these complex oxides needs also particular attention. In BSCF we have considered the defusing species as the perovskite ABO_3 unit with Ω = 1.60016x10^{-35} m^3 and N =1.5748x10^{23} mol.m^{-2}. In case of LN the diffusing species is La_2NiO_4 with Ω = 9.48049x10^{-35} m^3 and N = 4.8096x10^{22} mol.m^{-2}. Ω for the two materials were calculated from the lattice parameters obtained from the X-ray diffractions of the materials.

Plotting ln (w) against ln (t) gives a straight line, with a slope of about 1/4 implying that the dominant mass transport mechanism is surface diffusion.[23] If the slope of the plot is equal to 1/3 or 1/2 the mass transport is dominated by volume diffusion or evaporation condensation, respectively. In this region both surface diffusion and volume diffusion mechanisms are involved in the mass transport,[23] which requires correction for grain boundary groove width. Also by plotting w versus $t^{1/4}$ a straight line is obtained with a slope equals to $4.6B^{1/4}$, giving the value of B at a given annealing temperature. The surface diffusion coefficient at that temperature is then determined by using equation (2). The equation that relates surface diffusion coefficient to temperature is

$$Ds = D_s^o \exp\left(-\frac{E_a}{RT}\right) \qquad (3)$$

where D_s^o is the pre-exponential factor, E_a is the activation energy and R is the gas constant. By plotting the log of D_s as a function of the inverse temperature, the activation energy for surface diffusion is obtained from the slope.

During groove formation according to Mullins's model, grain boundary flux is assumed to be zero. Therefore the amount of matter that is removed from the grain boundary below the original surface is equal to the amount of matter deposited above the original surface upon groove formation.[24] The formation of grain boundary groove by surface diffusion is accompanied by an increase in depth of the groove with time $(t)^{1/4}$.[24,25] Apart from the power law dependence, different geometrical features of the groove profile account for different diffusion mechanisms. The absence of humps at the edge of a grain boundary groove implies that mass transport occurs mainly by evaporation – condensation[4,26] where the grain boundary groove forms but does not protrude above the original surface. The groove profile has no maxima/minima and the mass is not conserved. While mass is conserved in volume diffusion and surface diffusion, the former exhibit maxima but no minima while the latter exhibit both maxima and minima.[27]

Experimental

$La_2NiO_{4+\delta}$ (LN) and $Ba_{0.5}Sr_{0.5}Co_{0.8}Fe0.2O_{3-\delta}$ (BSCF) powders were synthesized by spray pyrolysis of nitrate solutions by CerPoTech AS (Trondheim, Norway). The BSCF powder was calcined for 24 h at 900 ºC, while the LN powder was calcined for 24 h at 800 ºC. After calcination the powders were ball-milled for 24 h using zirconia balls and isopropanol and dried over night to remove the solvent. Pellets 10 mm in diameter were prepared by uniaxial pressing using 60 MPa pressure, followed by cold isostatic pressing (CIP) using 200 MPa pressures. Sintering of the samples was conducted at 1300 ºC for 8 h and 1050 ºC for 12 h in air for LN and BSCF respectively, using heating and cooling rates of 200 ºC/ h. The sintered samples were polished using SiC paper, followed by a diamond paste down to 1 μm. The polished samples were cleaned in an ultrasonic bath using isopropanol, and dried in an oven at 80 ºC. The dense and polished samples were further thermally annealed in air at various time between 900 and 1100 ºC for LN and between 900 and 1020 ºC for BSCF, using heating and cooling rates of 10 ºC /min.

The phase purity of the materials was confirmed by powder X-ray diffraction using Bruker D8 Da Vinci 1 diffractometer. The density of the sintered samples was determined by Archimedes method. The microstructures of the polished as well as the thermally annealed samples were examined by scanning electron microscope (SEM, Hitachi S-3400N) equipped with an energy dispersive spectroscopy detector (EDS, X-MAX, Oxford Instruments). Measurement of surface profiles of the annealed samples was conducted by atomic force microscope (AFM, Veeco Multimode V) equipped with Nanoscope V controller, a high intensity illuminator and a video optical microscope. Microscope scanning was done by using Bruker J Scanner 10012 JVLR operated in contact mode in air, with a scan area capability of 160 x 160 μm. Scan rates of 0.6 Hz and scan areas between 3 x 3 and 30 x 30 μm^2 respectively were used. Groove profiles were analyzed from the AFM surface images by using *Nanoscope Analysis* software version 1.50. A line was drawn perpendicular to the grain boundary to measure the cross-sectional profile of the groove, and the grain boundary width was recorded as the distance between the two maxima as illustrated in Fig. 1. Fifty groove widths (*w*) were taken for every sample over about 4 – 6 AFM images, and the average grain boundary width for each sample was calculated. For each annealing temperature, the average value of a groove width w was plotted as a function of annealing time on a logarithmic scale.

Results

Representative SEM images of thermally annealed surfaces of the BSCF and LN ceramics are shown in Fig. 2. The average grain size of BSCF was 11.7 ± 1.9 and 15.9 ± 1.5 μm after annealing for 1 h at 900 and 980 ºC, respectively. Correspondingly, the average grain size of LN was 3.8 ± 0.3, and 4.3 ± 0.3 μm after annealing at 900 ºC for 1 h and 1100 ºC for 5 h, respectively. No grain growth could thus be observed for LN during thermal annealing at the conditions used in the study of grain boundary grooving, while a minor grain growth was observed for BSCF. We consider that this minor grain growth during the experiments does not have a significant influence on the surface diffusion data reported below.

Three-dimensional surface profiles measured by AFM of the thermally annealed BSCF and LN are shown in Fig. 3. An increase in the grain boundary width as a function of time is observed for both BSCF and LN. The grain boundary widths as well as the depths of the grain boundaries increased with thermal annealing time, thus it is evident that thermal development of the grain boundary grooves is in line with the predictions from the theory. The 3D surface profiles demonstrate that BSCF is isotropic and homogeneous, while the surface profile of LN shows the existence of different facets reflecting the anisotropic crystal structure of LN.

Two-dimensional profiles of the grain boundary groove of BSCF and LN are displayed in Fig. 4 at different annealing times and temperatures. The 2D profiles demonstrate an increasing grain boundary width and depth with annealing time. Mass transfer from the grain boundary towards the surface on both sides of the groove has clearly occurred during the thermal annealing, thus a clear first indication of surface diffusion mechanism. The thermal activation of the process is evident from Fig. 4c, demonstrating the strong temperature dependence of evolution of the grain boundary with at the same annealing time.

The evolution of the grain boundary groove width was determined from the AFM images for both ceramics as a function of the thermal annealing temperature and time. The data are summarized in Table 1 and 2. The data demonstrates that the width of the grain boundary groove increases with thermal annealing temperature and time in line with the expectation. The grain boundary groove width (w) is plotted as a function of time, $t^{1/4}$ according to eq. 1, in Fig. 5. All the data sets demonstrate a linear relationship with a slope (Table 1 and 2) corresponding to $4.6B^{1/4}$. The plots of ln (w) as a function of ln (t) at different thermal etching temperatures are shown in Fig. 6. A linear relationship is evident for both materials, with slopes close to ¼ for both materials as summarized in Table 1 and 2.

From B, calculated from the slopes in Fig. 5, the surface diffusion coefficient, D_s at different temperatures were calculated using the surface free energy and molecular volume as presented above. The resulting D_s is plotted in logarithmic form as a function of inverse temperature in Fig. 7. The activation energy for surface diffusion, determined by applying eq. 3, was found to be 450 ± 30 and 220 ± 30 k/Jmol for BSCF and LN, respectively.

The dihedral angle defined by the grain boundary grooves (Fig, 4) were found to be 151 ± 5 and 149 ± 8° for LN thermally annealed for 1 h at 950 °C and 1050 °C, respectively. For BSCF the dihedral angles were 157 ± 6, 156 ± 4 and 159 ± 3° respectively for samples that were thermally annealed for 1 h at 900, 940 and 980 °C. These results demonstrate that the dihedral angle is independent of temperature in the temperature range used here. This is also supported by the observation that as the annealing temperature/time increased, the grain boundary width and depth increased simultaneous keeping the dihedral angle constant. Finally, the observations of the dihedral angle also give support to that the surface energy is not strongly dependent on temperature.

Discussion

Prior to thermal annealing a thorough polishing of the sintered pellets was performed in order to obtain smooth surfaces sufficient to provide qualitative measures of the grain boundary grooving. Thermal annealing was conducted by using a rapid heating and cooling rate of 10 °C/min in order to minimize the contribution from the heating and cooling process to the dwell time, and therefore minimize the associated error of the grain boundary groove width. Fifty profiles of grain boundaries with uniform maxima were used to determine the grain boundary groove width, depth and dihedral angle for each annealing condition.

~~The grain boundary groove width, w, versus $t^{1/4}$, Fig. 5, for all the annealing temperatures is shown in Fig. 5 for LN and BSCF. A linear behavior is observed at all temperatures and the slope increases with temperature~~. The linear relationship shown in Fig. 5 demonstrates that mass transport occurs via surface diffusion, and the results agree well with the previously reports on other oxide materials.[28] According to Eq. 1, the slope of the plots equals to $4.6B^{1/4}$ from which B and hence the surface diffusion coefficient, D_s, is determined for each annealing temperature. The corresponding logarithmic plots, log w versus log t are shown in

Fig. 6 for LN and BSCF. The slopes determined by linear fit to the data (Table 1) are close to ¼, confirming that grain boundary grooving occurs through mass transport by surface diffusion. Temperature had no effect on the mass transport mechanism over the range of temperature studied, and only surface diffusion was responsible for mass transport and hence grain boundary grooving.

The surface diffusion data reported here are compared to similar data for other oxide materials in Fig. 8 (a). The slopes reflecting the activation energies (Table 4) and the range of the diffusion constants are comparable. The activation energies for BSCF, LN and Al_2O_3 are respectively higher and lower compared to the three other materials (UO_2, MnO, $CaTiO_3$). Normalizing the temperature with respect to the melting point of the compounds, see Fig. 8(b), the slopes become more comparable, reflecting that the mobility on the surface can be related to the melting point and thereby the bonding strength in the materials. This correlations has also been shown for bulk diffusion in oxides.[29]

The surface diffusion coefficient of LN is compared to diffusion of ions reported for LN in Fig. 9 (a) where diffusion coefficients for Ni^{2+}, Co^{2+}, La^{2+} and O^{2-} in LN are included. The diffusion coefficients of O^{2-} are significantly higher than the diffusion coefficients of cations in LN. The surface diffusion coefficient falls between the diffusion coefficient of O^{2-} and the cations. The surface diffusion coefficient constitutes the effective diffusion coefficient of the whole unit cell, including all the ions in the crystal structure. Only the effective surface diffusion coefficient is obtained by the grain boundary grooving approach, and is governed by the slowest moving specie at the surface. Diffusion of oxygen anions is by far the fastest process in the bulk, with diffusion coefficients about four orders of magnitude larger than the surface diffusion and ~7-8 orders of magnitude higher than the cation diffusion coefficients. Diffusion data for BSCF is less studied, but the relevant data reported is compared to the surface diffusion data in Fig. 9(b). Only data for oxygen anions and impurity diffusion of Mn and La cations are included.[10] The surface diffusion coefficient is significantly higher than the cation diffusion, with ~5 orders of magnitude difference. The extrapolated surface diffusion to lower temperatures falls between the oxygen anion and cation diffusion in line with the data for LN. These results demonstrate that at high temperature the mobility of cations on the surface in BSCF is exceptionally high, making the overall surface diffusion coefficient high.

Several factors could account for this observed behavior. One possible reason is the strength of ionic bonding in BSCF relative to other materials. Due to low ionic charge and small ionic size of the B-cations in the perovskite lattice, the ionic strength in BSCF is lower and therefore likely to cause weaker bonding strength. It is also likely that if the surface exhibits surface vacancies that enhance surface transport, this would affect the surface transport properties. In this case therefore, the difference in surface vacancies such as point defects would also account for the variation of surface diffusion coefficients, and hence the activation energy for diffusion.

We have compared the activation energy of surface diffusion with the corresponding activation energy of creep of the corresponding materials, reflecting either bulk or grain boundary diffusion (Table 5). In both the case of surface diffusion and creep the kinetics will be related to the slowest moving species in the unit cell since the whole unit cell need to migrate. The activation energy for creep seems to be to some degree higher than the corresponding activation energy for surface diffusion. This is also intuitively reasonable since the ions at the surface are under bounded compared to the ions in the bulk or at the grain boundaries.

The AFM images in Fig. 3 demonstrate that while the grains in BSCF are isotropic and homogeneous, those of LN are anisotropic and inhomogeneously thermally etched. The grain isotropy and anisotropy in the two materials reflects their crystallographic structures. BSCF exhibits a cubic perovskite structure, and LN is a first member in the Ruddlesden Popper series. The larger uncertainty in the slopes of ln w vs ln t for LN relative to BSCF is associated with the anisotropic crystallography of LN. The grain boundary groove width and depth increase with annealing time at constant temperature for both materials (Fig. 4). Similar behavior is observed for different annealing temperature but the same annealing time. Due to the crystallographic anisotropy and the crystallographic orientation of two adjacent grains caused a significantly variation in the morphology of the grain boundary groove and the dihedral angle. In our analysis, we have not made a more systematic study of how the dihedral angle and grain boundary groove width changed due to the anisotropy, and we have reported data assuming that LN is an isotropic material. The influence of crystallographic anisotropy is an interesting topic, which should be followed up in future studies.

Conclusion

Atomic Force Microscopy was successfully used to study the mass transport mechanism for grain boundary grooving in BSCF and LN materials. The development of the groove profiles was found to be in a reasonable agreement with the theory developed by Mullins. The grain boundary groove widths (w) were found to increase with thermal annealing temperature and time (t). A linear relationship between ln w vs ln t were observed with slopes close to ¼, demonstrating that surface diffusion was the dominant mass transport mechanism for grain boundary grooving. Surface diffusion coefficients for LN and BSCF at various thermal annealing temperatures were determined, and the activation energy for surface diffusion was determined. The activation energy for surface diffusion was found to be 450 ± 30 and 220 ± 30 kJ/mol for BSCF and LN respectively. Finally, the dihedral angle for LN and BSCF was determined by atomic force microscopy of the grain boundary grooves. The dihedral angle was observed to not depend significantly on temperature, and the angles observed are in the same range as reported for other oxide materials.

Acknowledgements

Financial support from the Research Council of Norway (RCN) through the CLIMIT program for SEALEM (project number 224918) is gratefully acknowledged.

References

1. G. Antczak and G. Ehrlich, "The beginnings of surface diffusion studies," *Surf. Sci.* **589**, 52-66 (2005).
2. H. Göbel and R. von Blanckenhagen, "A study of surface diffusion on gold with an atomic force microscope," *Surf. Sci.* **331-333**, 885-890 (1995).
3. W. M. Robertson, "Surface diffusion of oxides (A review)," *J. Nucl. Mater.,* **30**, 30-49 (1960).
4. M. Čeh and D Kolar, "Surface diffusion in $CaTiO_3$," *J. Mater. Sci.,* **24**, 4307 - 4310 (1989).
5. H. Göbel and R. von Blanckenhagen, "A study of surface diffusion on gold with an atomic force microscope," *Surf. Sci.* **331-333**, 885-890 (1995).
6. G. Ehrlich, "Direct observations of the surface diffusion of atoms and clusters," *Surf. Sci.,* **246**, 1-12 (1991).

7. R.C. Jaklevic and L. Elie, "Scanning-Tunneling-Microscope observation of surface diffusion on an atomic scale: Au on Au(111)," *Phys. Rev. Lett.* **60**, 120-124 (1988).
8. H.P. Hagan, P. A. Campbell, K.W. Smith, R.J. Turner and D.G. Walmsley, "Temporal behaviour of nanofeatures on Au,". *Ultr. Micr.* **42-44**, 587-593 (1992).
9. L. Kuipers and J. W. M. Frenken, "Jump to Contact, Neck Formation, and Surface Melting in the Scanning Tunneling Microscope," *Phys. Rev. Lett.* **70**, 3907-3911 (1993).
10. T. Suzuoka, "Mathematical Analysis of Tracer Surface Diffusion," *J. Phys. Soc. Jpn.* **20**, 1259-1270 (1965).
11. R. T. King and W. W. Mullins, "Theory of the decay of a surface scratch to flatness," *Act. Metall.,* **10**, 601-606 (1962).
12. Y. Kim and C. M. Lieber, "Machining oxide thin films with an atomic force microscope: Pattern and object formation on the nanometer scale," *Sci.,* **257**, 375-377 (1992).
13. T. A. Jung, A. Moser, H.J. Hug, D. Brodbeck, R. Hofer, H.R. Hidber and U.D. Schwarz, "The atomic force microscope used as a powerful tool for machining surfaces," *Ultr. Micr.* **42-44**, 1446-1451 (1992).
14. T. Maruyama and W. Komatsu, "Surface Diffusion of Single-Crystal Al_2O_3 by Scratch-Smoothing Method," *J. Amer. Ceram. Soc.* **58**, 338-339 (1975).
15. W. W. Mullins, "Theory of Thermal Grooving," *J. Appl. Phys.,* **28**, 333 - 339 (1957).
16. W. W. Mullins and P. G. Shewmon, "The kinetics of grain boundary grooving in copper," Act. Metall. **7**, 163 - 170 (1959).
17. M. G. Sahini, J. R. Tolchard, K. Wiik and T. Grande, "High temperature X-ray diffraction and thermogravimetrical analysis of the cubic perovskite $Ba_{0.5}Sr_{0.5}Co_{0.8}Fe_{0.2}O_{3-\delta}$ under different atmospheres," *Dalt. Trans.,* **44**, 10875–10881 (2015).
18. C. Frayret, A. Villesuzanne and M. Pouchard, "Application of density functional theory to the modeling of the mixed ionic and electronic conductor $La_2NiO_{4+\delta}$: Lattice relaxation, oxygen mobility, and energetics of frenkel defects". *Chem. Mater.*, **17**, 6538-6544 (2005).
19. J. Zhou, G. Chen, K. Wu and Y. Chen, "Interaction of La2NiO4 (100) Surface with Oxygen Molecule: A First-Principles Study," *J. Phys. Chem.,* C117, 12991-12999 (2013)
20. M.S.D. Read, M.S. Islam, G.W. Watson, and F.E. Hancock, "Surface structures and defect properties of pure and doped La_2NiO_4," *J. Mater., Chem.* 11, 2597-2602 (2001)
21. R. I. Eglitis, "Ab initio calculations of $SrTiO_3$, $BaTiO_3$, $PbTiO_3$, $CaTiO_3$, $SrZrO_3$, $PbZrO_3$ and $BaZrO_3$ (001), (011) and (111) surfaces as well as F centers, polarons, KTN solid solutions and Nb impurities therein,"*Int. J. Mod. Phys B*, 17, 1430009 (2014)
22. Read More: http://www.worldscientific.com/doi/abs/10.1142/S0217979214300096MMM
23. A. R. Gaddipati and W. D. Scott, "Surface mass transport of alumina," *J. Mater. Sc.,* **21**, 419-423 (1986).
24. P. Sachenko, "Experimental and simulated grain boundary groove profiles in tungsten," *Phil. Mag. Lett.*, **80**, 627- 631 (2000).
25. P.J. Goodhew and D. A. Smith, "Grooving at grain boundaries in thin films," *Scrip. Metall.,* **16**, 91-94 (1982).
26. M. I. Peters and I. E. Reimanis, "Grain boundary grooving studies of Yttrium Aluminium Garnet (YAG) bicrystals, *J. Am. Ceram. Soc.,* **86**, 870 - 872 (2003).
27. W. Zhang, P. Sachenko and I. Gladwell, "Thermal grain boundary grooving with anisotropic surface free energies," *Act. Mater.,* **52**, 107-116 (2004).
28. W. Shin, W.-S. Seo and K. Koumoto, "Grain-Boundary Grooves and Surface Diffusion in Polycrystalline Alumina Measured by Atomic Force Microscope," *J. Eur. Ceram. Soc.,* **18**, 595-600 (1998).
29. M. Palcut, K. Wiik and T. Grande, Cation self-diffusion in $LaCoO_3$ and La_2CoO_4 studied by diffusion couple experiments, J. Phys. Chem. B 111, 2299-2308 (2007).
30. W.M. Robertson and R. Chang, "The Role of Grain Boundaries and Surfaces in Ceramics," *Mater. Sc. Res.*, **3**, (ed W. W. Kriegel and H. Palmour) *Plenum Press, New York*, (1966).

31. W.M. Robertson and F.E. Ekstrom, " Kinetics of Reactions in Ionic Systems," *Mater. Sc. Res*., **4**, (ed T.J. Gray and V.D. Frechette) *Plenum Press, New York*, (1969).
32. P. Nikolopoulos, "Surface, grain-boundary and interfacial energies in Al_2O_3 and Al_2O_3-Sn, Al_2O_3-Co systems," J. Mater. Sc., **20**, 3993-4000 (1985).
33. D.M. Saylor and G.S. Rohrer, "Measuring the influence of grain-boundary misorientation on thermal groove geometry in ceramic polycrystals," *J. Am. Ceram. Soc.*, **82**, 1529-1536 (1999).
34. M. Jin, E. Shimada and Y. Ikuma, "Atomic Force Microscopy study of surface diffusion in polycrystalline CeO_2 via grain boundary grooving," *J. Ceram. Soc. Jap.*, **108**, 456-461 (2000).
35. J. Henney and J.W.S. Jones, "Surface-Diffusion Studies on UO_2 and MgO," *J. Mater. Sc.,* **3**, 158-164 (1968).
36. M.O. Marlowe and A.I. Kaznoff, " Tracer study of the surface diffusivity," *J. Nucl.Mater.,* **25**, 328-333 (1968).
37. J.B. Smith and Truls Norby, "On the Steady-State Oxygen Permeation Through $La_2NiO_{4+\delta}$ Membranes," *J. Electr. Soc.,* **153**, A233-A238 (2006).
38. S. J. Skinner and J.A. Kilner, "Oxygen diffusion and surface exchange in $La_{2-x}Sr_xNiO_{4+\delta}$," *Sol. Stat. Ion.,* **135**, 709-712 (2000).
39. N. Čebašek, R. Haugsrud, J. Milošević, Z. Li, J.B. Smith, A. Magrasó and T. Norby, "Determination of the Self-Diffusion Coefficient of Ni^{2+} in $La_2NiO_{4+\delta}$ by the Solid State Reaction Method," *J. Electr. Soc.,* **159**, B702-B708 (2012).
40. N. Čebašek, R. Haugsrud, Z. Li and T. Norby, "Determination of Chemical Tracer Diffusion Coefficients for the La- and Ni-site in $La_2NiO_{4+\delta}$ Studied by SIMS," *J. Am. Ceram. Soc.,* **96**, 598-605 (2013).
41. A. Berenov, A. Atkinson, J. Kilner, M. Ananyev, V. Eremin, N. Porotnikova, A. Farlenkov, E. Kurumchin, H.J.M. Bouwmeester, E. Bucher and W. Sitte, "Oxygen tracer diffusion and surface exchange kinetics in $Ba_{0.5}Sr_{0.5}Co_{0.8}Fe_{0.2}O_{3-\delta}$," *Sol. Stat. Ion.*, **268**, 102-109 (2014).
42. S.P. Harvey, R.A. De Souza and M. Martin, "Diffusion of La and Mn in $Ba_{0.5}Sr_{0.5}Co_{0.8}Fe_{0.2}O_{3-\delta}$ polycrystalline ceramics," *Ener. Envir. Sci.***, 5**, 5803 (2012).
43. A. Tsoga, D. Sotiropoulou and P. Nikolopoulos, "Grain boundary grooving in polycrystalline oxides and surface diffusion coefficient in polycrystalline alumina," *Mater. Sc. For.*, **207-209**, 565-568 (1996).
44. J. F. Shackelford and W.D. Scott, "Relative energy of [1100] tilt boundaries in aluminum oxide," *J. Am. Ceram. Soc*., **51**, 688 - 692 (1968).
45. B. Rutkowski, J. Malzbender, T. Beck, R.W. Steinbrech, and L. Singheiser, "Creep behaviour of tubular $Ba_{0.5}Sr_{0.5}Co_{0.8}Fe_{0.2}O_{3-\delta}$ gas separation membranes," *J. Eur. Cer. Soc.,* **31**, 493-499 (2011).
46. J.X. Yi, H. L. Lein, T. Grande, S. Yakovlev and H.J.M. Bouwmeester, "High-temperature compressive creep behaviour of the perovskite-type oxide $Ba_{0.5}Sr_{0.5}Co_{0.8}Fe_{0.2}O_{3-\delta}$," *Sol. Stat. Ion.,* **180**, 1564-1568 (2009).
47. A. Crosby and P.E. Evans, "Creep in pure and two phase nickel-doped Alumina," *J. Mater. Sc.,* **8**, 1573-1580 (1973).
48. P. Li, S.-I Karato and Z. Wang, "High-temperature creep in fine-grained polycrystalline $CaTiO_3$, an analogue material of (Mg, Fe)SiO_3 perovskite," *Phys. Earth. Plan. Inter.,* **95**, 19-36 (1996).
49. S. Mei, D. L. Kohlstedt, W.B. Durham and L. Wang, "Experimental investigation of the creep behavior of MgO at high pressures," *Phys. Earth. Plan. Inter.,***170**, 170-175 (2008).
50. R. C. Bradt and R. E. Tressler, "*Deformation of Ceramic Materials," Plenum Press*, **271**, (1975).
51. T. G. Desai, P.C. Millett and D. Wolf, "Molecular dynamics study of diffusional creep in nanocrystalline UO_2," *Act. Mater.,* **56**, 4489-4497 (2008).

Tables

Table 1
Average groove widths for LN at various thermal annealing temperatures and times. Slope 1 is the slope of w vs $t^{1/4}$, and slope 2 is the slope of ln w vs ln t. S.D = Standard deviation.

LN				
T (ºC)	t (s)	w ± S.D (μm)	Slope 1 (± S.D)	Slope 2 (± S.D)
900	3600	0.22 ± 0.05	0.03	0.27
	18000	0.33 ± 0.06	± 0.01	± 0.06
	43200	0.44 ± 0.06		
	86400	0.52 ± 0.08		
950	3600	0.36 ± 0.04	0.04	0.23
	18000	0.48 ± 0.04	± 0.02	± 0.07
	43200	0.64 ± 0.06		
	86400	0.70 ± 0.12		
1000	3600	0.50 ± 0.07	0.06	0.22
	18000	0.73 ± 0.11	± 0.02	± 0.09
	43200	0.89 ± 0.15		
	86400	1.00 ± 0.12		
1050	3600	0.58 ± 0.09	0.06	0.23
	18000	0.81 ± 0.10	± 0.03	± 0.12
	43200	0.98 ± 0.10		
1100	3600	0.62 ± 0.10	0.07	0.19
	18000	0.91 ± 0.14	± 0.04	± 0.13
	43200	1.11 ± 0.17		

Table 2
Average groove widths for BSCF at various thermal etching temperatures and times. Slope 1 is the slope of w vs $t^{1/4}$, and slope 2 is the slope of ln w vs ln t. S.D = Standard deviation.

T (ºC)	t (s)	w ± S.D (μm)	Slope 1 (± S.D)	Slope 2 (± S.D)
900	900	0.89 ± 0.10	0.12	0.22
	3600	1.12 ± 0.15	± 0.04	± 0.05
	18000	1.51 ± 0.10		
	43200	2.08 ± 0.15		
940	900	1.27 ± 0.11	0.15	0.20
	3600	1.52 ± 0.11	± 0.05	± 0.06
	18000	2.24 ± 0.22		
	43200	2.70 ± 0.28		
980	900	1.76 ± 0.19	0.24	0.21
	3600	2.16 ± 0.21	± 0.08	± 0.05
	18000	3.21 ± 0.33		
	43200	3.89 ± 0.42		
1020	900	2.61 ± 0.12	0.35	0.20
	3600	3.31 ± 0.18	± 0.09	± 0.05
	18000	4.74 ± 0.28		

Table 3

Dihedral angles of grain boundary grooves of thermally annealed BSCF and LN measured by AFM.

Temp. (K)	Material	Dihedral angle °(Ψ)	Ref.
1223	**LN**	151 ± 5	This work
1323		149 ± 8	
1173	**BSCF**	157 ± 6	This work
1213		156 ± 4	
1253		159 ± 3	
1643	Al_2O_3	147	[28]
1723		129	
1803		124	
1873		118	
1873	Al_2O_3	115	[30]
1873	MgO doped Al_2O_3	117	
1673	MgO doped Al_2O_3	130	[31]
1473	Al_2O_3 +Sn (metal)	146	[32]
1623	Al_2O_3 +Sn (metal)	145	
1783	Al_2O_3 +Co (metal)	159	
1923	Al_2O_3 +Co (metal)	158	
1673	MgO	105	[33]
1873	Al_2O_3	106	
1473	CeO_2	161	[34]
1543		160	
1603		156	
1663		154	

Table 4
The activation energies for surface diffusion measured from grain boundary grooves for various materials.

Material	Technique	Temp. (K)	E_a (kJ/mol)	Ref.
$CaTiO_3$ (P)	GBV, SA	1473 – 1773	330 ± 30	[4]
Al_2O_3(P), 99.7 %	GBV, O.I	1273 – 1736	256	[43]
Al_2O_3(P), 99.7 %	GBV, O.I	1373 – 1993	314	[30]
Al_2O_3(P), 99.7 %	GBV, AFM	1643 – 1873	577	[28]
High purity Al_2O_3 (S)	GBV, O.I	1673 – 1973	544	[31]
High purity Al_2O_3(S)	GBV, O.I	1773 – 2273	452	[23]
MgO		1443 – 1770	370	[35]
UO_2, Dry H_2		1573 – 1973	380	[35]
UO_2, Ar		1473 – 1873	320	[35]
UO_2		1823 – 2193	505	[36]
Al_2O_3(B)	S.T, GBV,O.I	1813 – 2013	460	[44]
BSCF	GBV, AFM	1173 – 1293	450 ± 30	This work
LN	GBV, AFM	1173 – 1373	220 ± 30	This work

Table 5

The activation energy for creep for various oxide materials, together with the activation energy for surface diffusion from this work.

Material	**Grain size (µm)**	**Temp. (K)**	**E_a (kJ/mol)**	**Ref.**
BSCF		1173 – 1293	450 ± 30	This work
LN		1173 – 1373	220 ± 30	This work
BSCF		>1123,heating	530	[45]
BSCF		>1123,cooling	340 ± 40	[45]
BSCF		1078 - 1208	> 250	[46]
Al_2O_3	15	1750 - 2000	431 ± 50	[47]
	21	1750 - 2000	456 ± 25	
	45	1750 - 2000	472 ± 13	
$CaTiO_3$	8.2	1440 - 1490	731	[48]
	27.3	1470 - 1515	803	
MgO		1350 - 1590	72	[49]
Al_2O_3		1623 - 1798	540 ± 20	[50]
UO_2			372 ± 5	[51]

Figure captions

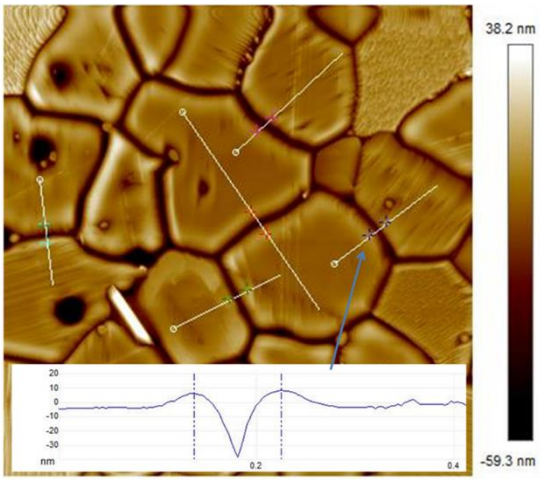

Figure 1
The surface profile of thermally annealed sample and the cross – section of the grain boundary, indicating how the width of the grain boundary groove is determined.

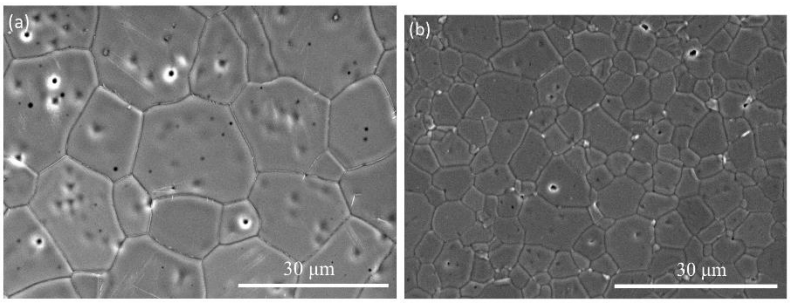

Figure 2

SEM (SE) images of polished surfaces of (a) BSCF annealed at 940 ºC for 1 h and (b) La_2NiO_4 annealed at 1100 ºC for 5 h.

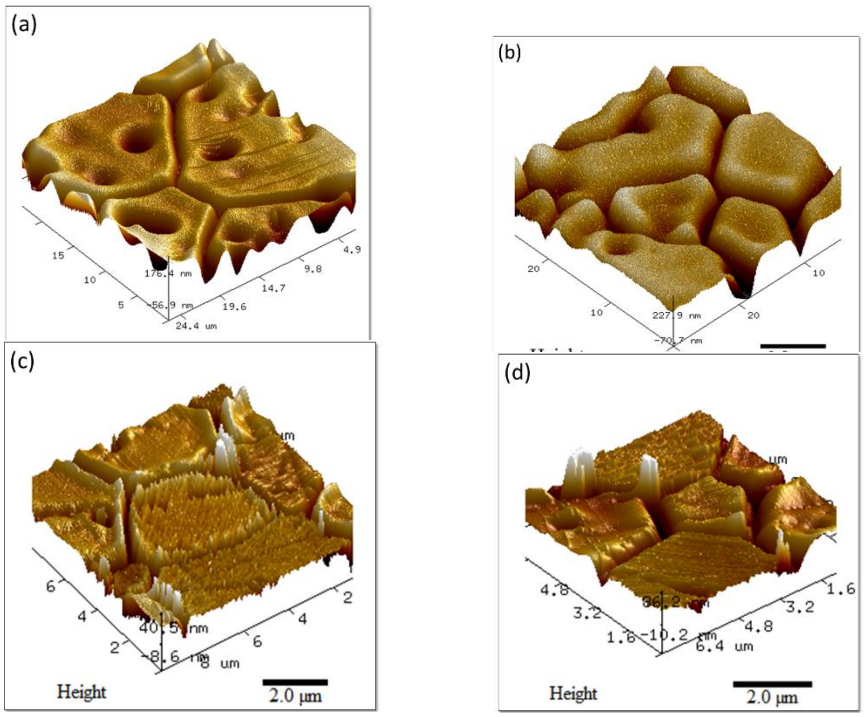

Figure 3
Three-dimensional AFM surface profiles of BSCF thermally annealed at 980 ºC for 1 h (a) and 5 h (b), and LN thermally annealed at 1000 ºC for 1 h (c) and 12 h (d).

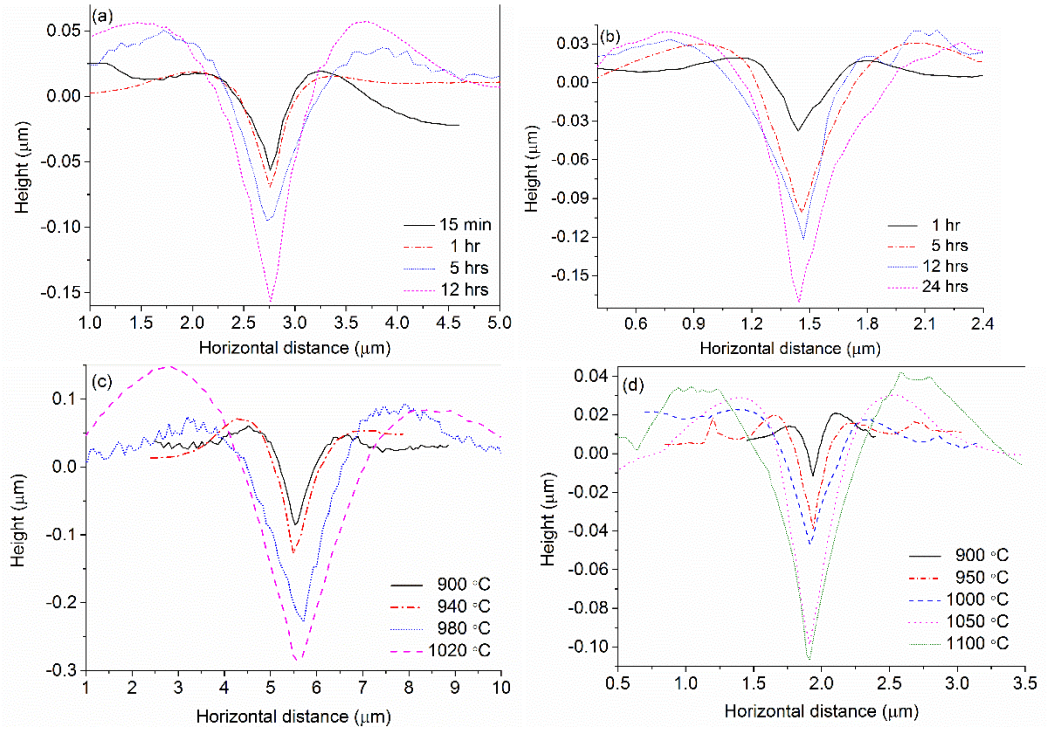

Figure 4
The grain boundary groove profiles of BSCF at 900 ºC (a) and LN at 1050 ºC (b) as a function of time. c) The grain boundary groove profiles of BSCF after 5 h at different temperatures.

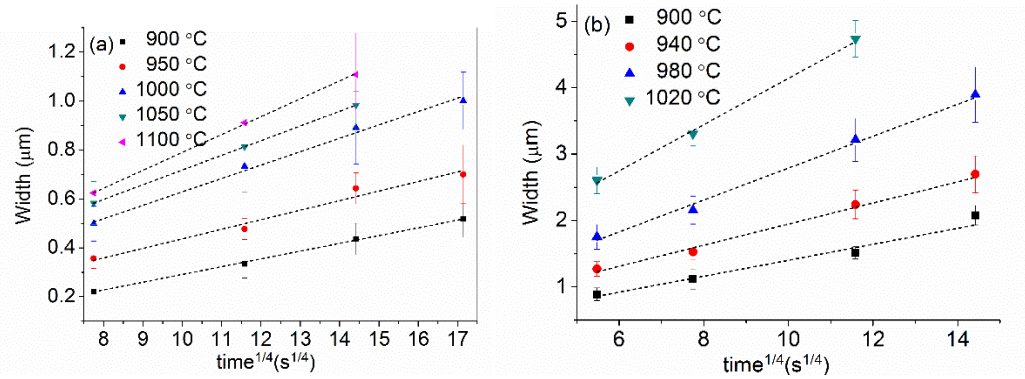

Figure 5
Grain boundary width w, as a function of time, $t^{1/4}$ for LN (a) and BSCF (b).

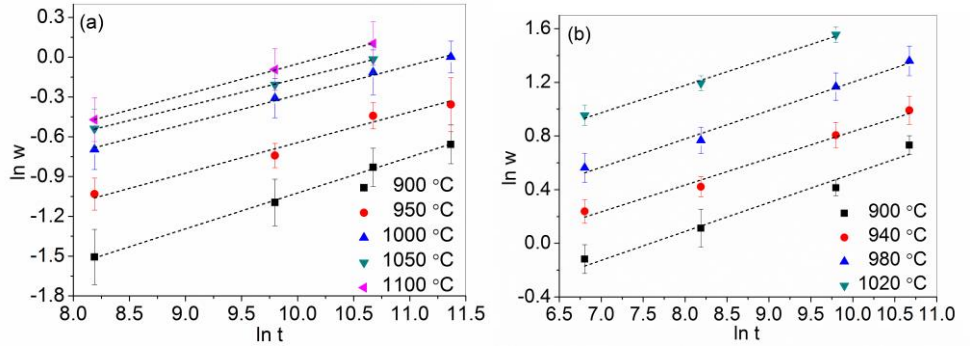

Figure 6
ln (w) as a function of ln (t) for and La_2NiO_4 (a) BSCF (b), thermally etched at various temperatures**.**

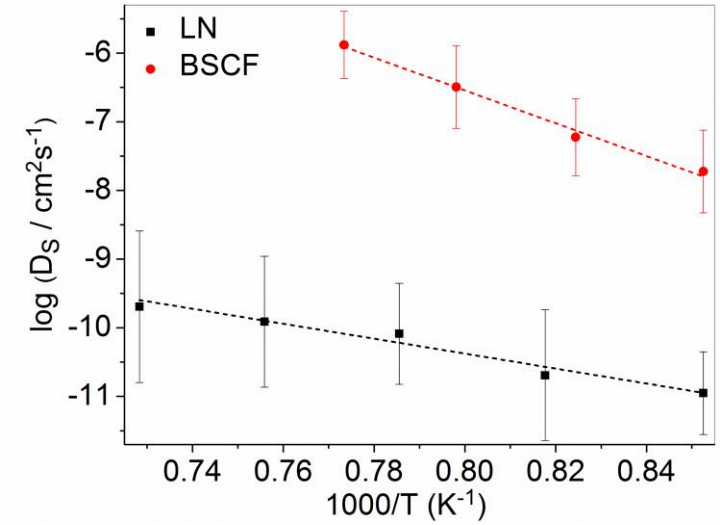

Figure 7
The logarithm of D_s as a function of 1/T for BSCF, and LN at various thermal annealing temperatures and time

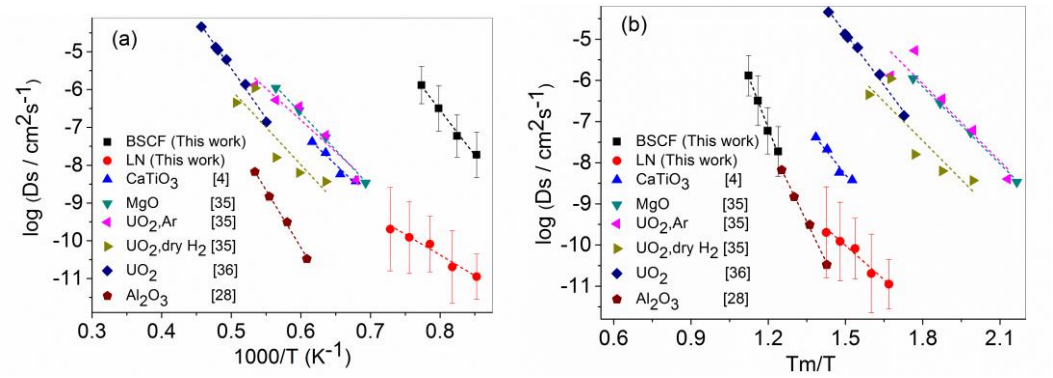

Figure 8
The logarithm of D_s as a function of inverse temperature for BSCF, and LN at various thermal annealing temperatures, together with surface diffusion data reported for various oxides.[4,28,35,36]

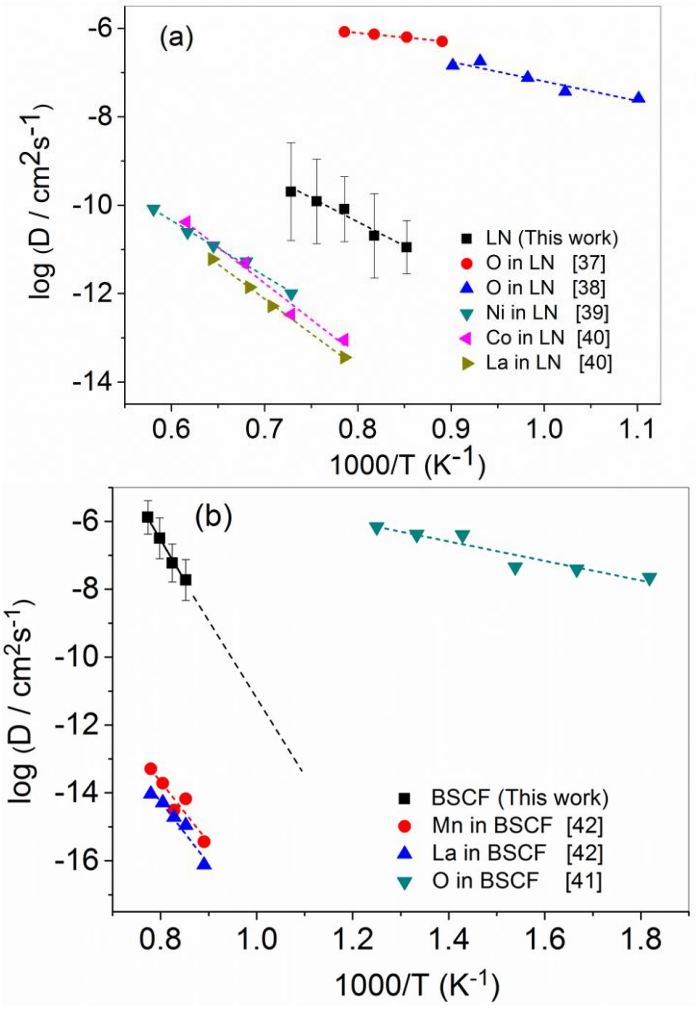

Figure 9
Diffusion data on logarithmic scale as a function of 1/T for LN (a) and BSCF (b) at various thermal annealing temperatures, together with reported oxygen and cation bulk diffusion data.[37-42]

-